WARSAW UNIVERSITY OF TECHNOLOGY Index 351733
FACULTY OF CIVIL ENGINEERING
COMMITTEE FOR CIVIL AND WATER ENGINEERING
POLISH ACADEMY OF SCIENCES ISSN 1230-2945

DOI: 10.24425/ace.2020.131787

ARCHIVES OF CIVIL ENGINEERING

Vol. LXVI ISSUE 1 2020

PROGNOSIS OF DYNAMIC BEHAVIOR OF REINFORCED CONCRETE DEEP BEAMS OF VERY HIGH STRENGTH MATERIALS

W. CICHORSKI[1], A. STOLARSKI[2]

Abstract. An analysis of the dynamic load - carrying capacity of rectangular reinforced concrete deep beam considering the physical nonlinearities of structural materials: concrete and reinforcing steel, is the aim of the paper. The model of the elastic/visco-perfectly plastic material including dynamic yield criterion was applied for the reinforcing steel. The non-standard model of dynamic deformation, regarding the dynamic strength criterion and material softening was applied for the concrete. The method for description of deformation parameters of high strength concrete was included in the model. The method of structure effort analysis was developed using the finite element method. The comparative analyses of the obtained results for three different values of high strengths of concrete and one value of high yield stress for reinforcing steel were carried out in relation to the numerical results obtained for ordinary concrete and steel in case of dynamic loading. In these cases, the significant differences in behavior of reinforced concrete deep beams have been observed and described in detail. The effectiveness of the method analysis and computational algorithms for the problems of numerical simulation of reinforced concrete deep beam dynamic behavior was indicated in the paper.

Keywords: structural mechanics, reinforced concrete structures, deep beam, dynamic load, physical nonlinearity

[1] PhD., Eng., Military University of Technology, Faculty of Civil Engineering and Geodesy, 2 Kaliskiego Str., 00-908 Warsaw-49, Poland, orcid.org/0000-0002-0481-2343, e-mail: waldemar.cichorski@wat.edu.pl

[2] Prof., DSc., PhD., Eng., Military University of Technology, Faculty of Civil Engineering and Geodesy, 2 Kaliskiego Str., 00-908 Warsaw-49, Poland, orcid.org/0000-0002-4754-3067, e-mail: adam.stolarski@wat.edu.pl

1. INTRODUCTION

Specific features of high performance concretes cause the necessity to undertake not only the experimental investigations but also theoretical research in the area of modelling the constitutive materials properties, modelling the behavior of plain concrete and reinforced concrete structures as well as the analysis of effort and damage mechanisms of structures made from such concretes. An example of such an analysis is the solution concerning the influence of high strength of concrete and reinforcing steel on behavior of reinforced concrete deep beam in the range of static loadings [7]. The solution was obtained on the base of the method of analysis of inelastic behavior of the reinforced concrete deep beam under static load [3, 8]. The analysis of static load carrying capacity of reinforced concrete deep beam was determined in the process of incremental loading. In these papers the comparative analysis of the results was carried out with experimental results taken from the literature [5], as well as with the previous numerical results [4], obtained for ordinary concrete. In these analyses, the results of numerical solutions were presented with comparison to the experimental results and other numerical results taken from the literature for static loading showing very good agreements in the range of the load - carrying capacity and the displacement state analysis.

Various concrete models function in the literature. Detailed information is provided in [12]. Other models of dynamic behavior of concrete and its cracking, considering plastic damage, can be found in e.g. [13, 14].

The purpose of the paper is the analysis of influence of very high strength concrete and reinforcing steel on the behavior of reinforced concrete deep beam during the process of dynamic deformation. Obtaining the solutions requires making investigations in the range of the modelling dynamic, inelastic material properties, modelling of deformation processes of the plane structural element – reinforced concrete deep beam, and preparing numerical solutions.

Modelling of structural material properties was carried out using the dynamic material models. The modified model of the elastic/visco-perfectly plastic material regarding delayed yield effect, was applied for the reinforcement steel [1]. The model of dynamic deformation was applied for the concrete [9, 12]. The basis of this model is the method of determination the initial dynamic yield surface. For this purpose, the structure of Campbell's dynamic yield criterion, was used [2]. Proposed criterion is an integral condition of attaining the dynamic strength [10]. The calculated dynamic strength is treated as a parameter in the constitutive equations, which describes the elastic-

plastic model of concrete. The model describes the effect of increase of the dynamic strength in proportion to static strength, limited perfectly plastic properties of concrete, material softening and material dilatation in the straining process. The model makes it possible the simplified description of cracking or crushing of material as the states of loss of load-capacity, which are reached in the material softening process during tension or compression. Introduction of the additional modification of material parameters allows the description of the properties of very high strength concrete.

Selected results of the numerical solutions were presented in the paper. The comparative analyses of the obtained results for three different values of high strengths of concrete and one value of high yield stress for reinforcing steel were carried out in case of dynamic loading.

2. DYNAMIC MODEL OF REINFORCEMENT STEEL

The modified model of elastic/visco-perfectly plastic material taking into consideration the delayed yield effect, was employed to dynamic analysis [1]. Considering the functioning of the deep beam's reinforcement as slender steel bars, material model in uniaxial stress state, was applied to the reinforcement steel. In this model, Perzyna's constitutive equations of elastic-viscoplasticity [6], can be written in the form:

$$\dot{\varepsilon} = \frac{\dot{\sigma}}{E_s} + \tilde{\gamma} < \Phi(F) >, \quad \tilde{\gamma} = \frac{2}{\sqrt{3}}\gamma, \tag{2.1}$$

where: E_s - modulus of elasticity; γ - viscosity coefficient.

The modification of Perzyna's constitutive equations is based on the integration those equations with initial condition as the dynamic yield limit, which is determined on the base of Campbell's dynamic yield criterion [2], in the form:

$$\int_0^{t_d} [\frac{\sqrt{\sigma(t)}}{f_y}]^{\alpha} dt = t_0 \tag{2.2}$$

where: α and t_0 - material constants; f_y - tensile / compressive static yield limit of steel; $\sigma(t)$ – variable stress over time.

At the time instant of satisfy the Campbell's criterion, time of the delayed yielding $t = t_d$ and dynamic yield limit $f_{yd} = \sigma(t_d) \geq f_y$, are determined.

Static yield function for the elastic-perfectly plastic material, has the form:

$$F = \frac{\sigma}{f_y} - 1 \tag{2.3}$$

Symbol $< \Phi(F) >$ is defined as follows:

$$< \Phi(F) >= \begin{cases} 0 & for \quad t \leq t_d \\ \Phi(F) \quad if \quad F > 0 & for \quad t > t_d \\ 0 \quad if \quad F \leq 0 & \end{cases} \tag{2.4}$$

Nonlinear function $\Phi(F)$, was assumed in the form of a power law:

$$\Phi(F) = F^{\delta} \tag{2.5}$$

where: δ - material coefficient.

Dynamic yield condition, has the form:

$$\sigma = f_y[1 + (\frac{\sqrt{\dot{\varepsilon}^{vp}}}{\tilde{\gamma}})]^{1/\delta} \tag{2.6}$$

where: $\dot{\varepsilon}^{vp}$ - viscoplastic strain rate.

3. DYNAMIC MODEL OF CONCRETE

The non-standard model of the dynamic deformation of the concrete was applied to the dynamic analysis [9, 12]. The basic elements of the model are presented below.

$$F(\sigma_{ij}, K) = [\frac{\tau_0}{\rho(\phi)} + Ka]^2 - Kb\sigma_0 - K^2 c = 0 \tag{3.1}$$

where: τ_0 - tangent octahedral stress; σ_0 - mean normal stress; $\rho(\phi)$ - function determining the shape of the limit surface cross-section by the octahedral plane $\sigma_0 = const$; K – evolution parameter; $a,\ b,\ c$ - material constants, determined on the base of static strengths of concrete for uniaxial and biaxial compression and uniaxial tension for $K = 1$.

The basis of the model is the method of attaining the initial dynamic yield surface. For this purpose, the integral criterion of the dynamic strength for concrete in complex stress states, was used [10]:

$$\int_0^{t_d}[\psi(t)]^{\alpha_c}dt = t_{c0} \tag{3.2}$$

where: $\psi(t)$ is determined on the base of limit surface equation (3.1)

$$\psi(t) = \frac{2[\frac{\tau_0}{\rho(\phi)}]^2}{2a\frac{\tau_0}{\rho(\phi)} - b\sigma_0}\left\{\sqrt{1 - \frac{4(a^2-c)[\frac{\tau_0}{\rho(\phi)}]^2}{[2a\frac{\tau_0}{\rho(\phi)} - b\sigma_0]^2}} - 1\right\}^{-1} \tag{3.3}$$

and α_c, t_{c0} - material constants, which are determined on the base of experimental results for concrete.

At the time instant of satisfy the criterion of dynamic strength (3.2), time of attaining the dynamic strength $t = t_d$ and dynamic strength coefficient of concrete $\psi_d = \psi(t_d) \geq 1$, are determined.
Properties of the limit surface, especially its good agreement with experimental results for concrete in complex stress states, give the reason for applying Eq. (3.1) as a yield surface for the elastic-plastic material.
Parameter K, which scales the basic strength of the concrete, is interpreted as the parameter of the yield surface evolution. The following relation defines evolution parameter:

$$K_n = \begin{cases} 1 & & t_n < t_d \\ \psi_d & \varepsilon_{ef}^p \leq \varepsilon_{fc}^p & t_n \geq t_d \\ \psi_d + \int_{t_R}^{t_n}\dot{K}(\tau)d\tau \cong K_{n-1} + \dot{K}_n\Delta t & K_n \geq K_{min} \quad \varepsilon_{ef}^p > \varepsilon_{fc}^p & t_n > t_d \\ 0 & K_n < K_{min} \quad \varepsilon_{ef}^p > \varepsilon_{fc}^p & t_n > t_d \end{cases} \tag{3.4}$$

where: ε_{ef}^p - effective plastic strain; ε_{fc}^p - limit plastic strain in the perfectly plastic flow phase, n- number of time instant.

Applied definition of the evolution parameter K describes three-phase idealisation of the concrete behaviour. The following deformation phases are distinguished in this idealisation: 1° elastic attaining initial yield surface; 2° perfectly plastic flow in limited range of deformation; 3°° material softening modelled as a plastic flow on the transient yield surface, which isotropic shrinkage process is controlled by variation $\dot{K}$ of the evolution parameter, depended on effective plastic strain rate and softening modulus and modified in dependence on up-to-date stress state.
The following relation describes variation $\dot{K}$ of the evolution parameter:

(3.5) $$\dot{K}_n = \begin{cases} 0 & \varepsilon_{ef}^p \leq \varepsilon_{fc}^p \\ \psi_d H(\sigma_i^0)\dot{\varepsilon}_{ef}^p & \varepsilon_{ef}^p > \varepsilon_{fc}^p \end{cases}$$

where: $\dot{\varepsilon}_{ef}^p$- effective plastic strain rate; $H(\sigma_i^0)$ - material softening modulus.

Nondimensional material softening modulus has the form:

(3.6) $$H(\sigma_i^0) = -\frac{1}{\sigma_i^0(\varepsilon_{uc}-\varepsilon_{fc}+\psi_d\frac{f_c}{E_c})}$$

where: $\sigma_i^0 = \sigma_i/\psi_d$ - nondimensional stress intensity related to initial yield surface; ε_{fc} and ε_{uc} - limit plastic strains; E_c - modulus of elasticity; f_c - uniaxial compressive strength of concrete.

Tensor of the plastic strain increment is defined by postulating of non-associated flow rule:

(3.7) $$\dot{\varepsilon}_{ij}^p = \dot{\Lambda}\frac{\partial G}{\partial \sigma_{ij}}$$

where: G - plastic potential function; $\dot{\Lambda}$ - loading parameter.

Plastic potential function G was assumed in the form of a modified yield surface function:

(3.8) $$G(\sigma_{ij}, K) = [\frac{\tau_0}{\rho(\phi)} + Ka]^2 - K\frac{b}{\beta}\sigma_0 - K^2 c = 0$$

where: β - material constant defining of volumetric variation of the material during plastic deformation.

Linear-elastic material properties are described by generalized Hooke's law, which considering the strain increments decomposition and flow rule, can be written in the form:

(3.9) $$\dot{\sigma}_{ij} = C_{ijkl}\dot{\varepsilon}_{kl}^e = C_{ijkl}(\dot{\varepsilon}_{kl} - \dot{\varepsilon}_{kl}^p) = C_{ijkl}(\dot{\varepsilon}_{kl} - \dot{\Lambda}\frac{\partial G}{\partial \sigma_{kl}})$$

where: C_{ijkl} - elastic constants tensor.

Loading parameter is determined on the base of the relation:

(3.10) $$\dot{\Lambda} = \frac{\frac{\partial F}{\partial \sigma_{ij}}C_{ijkl}\dot{\varepsilon}_{kl}}{\frac{\partial F}{\partial K}A(\psi_d, H, \eta_{ef}) + \frac{\partial F}{\partial \sigma_{ij}}C_{ijkl}\frac{\partial G}{\partial \sigma_{kl}}}$$

where: $A(\psi_d, H, \eta_{ef}) = -\psi_d H(\sigma_i^0)\eta_{ef}(\frac{\partial G}{\partial \sigma_{ij}})$.

Loading and unloading processes are defined in the following way:

$$\begin{array}{rlllllll} \text{loading:} & \dot{\Lambda} > 0 & \text{if} & F = 0 & & & \text{and} & \dot{F} = 0 \\ \text{unloading:} & \dot{\Lambda} = 0 & \text{if} & F < 0 & \text{or} & F = 0 & \text{and} & \dot{F} < 0 \end{array} \tag{3.11}$$

Applied deformation model of concrete enables the simplified modelling of cracking or crushing mechanisms (i.e. formation, opening and closing of the cracks), both in the monotonic deformation processes as well as in the cyclic, alternating deformation processes. Cracking or crushing mechanisms of concrete result from employed softening rule, which assumes gradually loss of material load-capacity till the attaining of the stress-free state during tension or compression processes, respectively.

Considering the high strength concrete in the numerical analysis of deep beams, the modification of the concrete deformation model is proposed. The change of interpretation of limit strains ε_{fc} for the perfectly plastic flow phase and ε_{uc} for the material softening phase of deformation, is the essence of proposed modification of the model for concrete.

In the basic version of the model, the limit strain ε_{fc} is taken on the base of the analysis of experimental results for uniaxial compression tests as the constant values $\varepsilon_{fc} = 2‰$ independently from the grade of concrete. In turn, for the limit strain ε_{uc} the interval $\varepsilon_{uc} = (6 \div 12)‰$ is given, recommending the lower value of ε_{uc} for high-grade concrete and higher value of ε_{uc} for the low-grade and mean-grade concrete but without any precise determination of the dependency on the grade of concrete.

Now, in the modified version of concrete model, it is assumed that the values of limit strains ε_{fc} and ε_{uc} might be variable and dependent on the grade of concrete, according to the following function of strength variability of concrete determined so called strength indicator:

$$r(f_c) = \frac{f_c - f_{\mathrm{c,min}}}{\Delta f_c} \tag{3.12}$$

where: f_c - compressive strength of concrete is taken from the range ($f_{\mathrm{c,min}}$, $\mathrm{f_{c,max}}$), and $\Delta f_c = f_{\mathrm{c,max}} - f_{\mathrm{c,min}}$ is the length of compressive strength range.

Finally, the following relationships of limit strains are introduced:

- for the perfectly plastic flow phase:

$$\varepsilon_{\mathrm{fc}} = \varepsilon_{\mathrm{ec}} + \varepsilon_{\mathrm{fc,p}} \quad , \quad \varepsilon_{\mathrm{fc,p}} = \varepsilon_{\mathrm{fc,p,max}} - \Delta\varepsilon_{\mathrm{fc,p}} \cdot r(f_c) \, , \tag{3.13}$$

- for the material softening phase:

(3.14) $$\varepsilon_{\mathrm{uc}} = \varepsilon_{\mathrm{fc}} + \varepsilon_{\mathrm{fc,u}} \quad , \quad \varepsilon_{\mathrm{fc,u}} = \varepsilon_{\mathrm{fc,u,max}} - \Delta\varepsilon_{\mathrm{fc,u}} \cdot r(f_c) \ ,$$

where: $\varepsilon_{\mathrm{ec}} = \psi_d \frac{f_c}{E_c}$ - maximum elastic strain according to the assumed model of concrete;

$\Delta\varepsilon_{\mathrm{fc,p}} = \varepsilon_{\mathrm{fc,p,max}} - \varepsilon_{\mathrm{fc,p,min}}$ - the length of the limit strain range for the perfectly plastic flow phase;

$\Delta\varepsilon_{\mathrm{fc,u}} = \varepsilon_{\mathrm{fc,u,max}} - \varepsilon_{\mathrm{fc,u,min}}$ - the length of the limit strain range for the material softening phase.

To determine the material parameters describing the constitutive model of concrete, the following limit values were adopted:

$\varepsilon_{\mathrm{fc,p,min}} = 0.5$ ‰ and $\varepsilon_{\mathrm{fc,p,max}} = 0.8$ ‰ - minimum and maximum strains determining the range of the perfectly plastic flow phase,

$\varepsilon_{\mathrm{fc,u,min}} = 4$ ‰ and $\varepsilon_{\mathrm{fc,u,max}} = 10$ ‰ - minimum and maximum strains determining the range of the material softening phase, and

$f_{\mathrm{c,min}} = 30\ MPa$ and $f_{\mathrm{c,max}} = 300\ MPa$ - minimum and maximum compressive strengths of concrete.

As a result, the material parameters describing the constitutive model of concrete were considered for the numerical analysis, as presented in Table 1.

Table 1: Parameters describing the model of concrete

No.	Grade of concrete	f_c [MPa]	f_t [MPa]	ε_{ec} [‰] $\psi_d = 1$	ε_{fc} [‰]	ε_{uc} [‰]	E_c [GPa]
1	C30	30	3	1.20	2.00	12.00	25.0
2	C100	100	10	2.08	2.80	11.25	48.0
3	C200	200	20	3.88	4.49	10.71	51.5
4	C300	300	30	5.71	6.21	10.21	52.5

Graphical interpretation of the material parameters describing the constitutive model of concrete is shown in Figure 1, in the stress - strain plane for uniaxial compression and for $\psi_d = 1$.

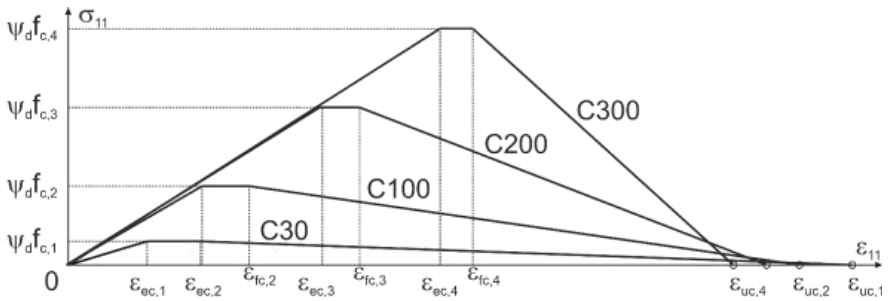

Fig. 1. Interpretation of material parameters describing constitutive model of concrete

4. METHOD OF ANALYSIS

4.1. GENERAL DESCRIPTION OF THE METHOD

The method of structure analysis is based on: 1^{O} discretization and description of the structure according to the finite element method principles; 2^{O} formulation of the system of the incremental equilibrium equations; and 3^{O} elaboration of own algorithms and procedures of numerical analysis of the plane stress state problem, which enable the determination of the displacement, strain, and non-linear stress fields, both in reinforcement steel and concrete.

4.2. DISCRETE MODEL OF REINFORCED CONCRETE STRUCTURE

The discretization of the structure using FEM is based on the following assumptions.

1^{O} Structure was divided into the finite elements of the matrix material (concrete) and of the reinforcement bars material (slender steel bars discretely distributed in the matrix material).

2^{O} Natural for reinforced concrete structures hypothesis of the interaction between concrete and reinforcement steel was applied under the assumption of perfect consistency of the displacements of both materials.

The matrix material was divided into rectangular elements. Four-node elements with two degrees of freedom in each node were applied. A fine mesh was used in the regions in which concentration of stresses was expected.

The reinforcement steel bars were modelled as linear bar elements. Two-node elements with two degrees of freedom in each node were used.

In turn, the principle of concrete and reinforcement steel bars interaction is realized in the following way.

1^{O} Two types of nodes are introduced:

- the main element nodes, respectively to the applied structure discretization, distinguishing between the nodes of the matrix material elements and the nodes of the reinforcement bar material elements,
- the common nodes of the matrix material elements and the reinforcement bar material elements as selected from among the main nodes.

2^{O} Displacement equivalence condition is introduced in the main nodes exclusively.

3^{O} Computational Gauss points on the matrix material element area are introduced.

4.3. SYSTEM OF EQUILIBRIUM EQUATIONS

The governing equation system for the solution of the dynamic problem of a reinforced concrete deep beam is determined in the following matrix and incremental form:

$$\boldsymbol{M}\ddot{\boldsymbol{r}}_{t+\Delta t} + \boldsymbol{K}\Delta\boldsymbol{r}_{t,t+\Delta t} = \boldsymbol{R}_{t+\Delta t} - \boldsymbol{F}_t \tag{4.1}$$

where: $\boldsymbol{M}$ - mass matrix, $\boldsymbol{K} = \boldsymbol{K}_c + \boldsymbol{K}_s$ - elastic stiffness matrix which has the additive form consisting of stiffness matrices for concrete elements $\boldsymbol{K}_c$ and for reinforcement steel elements $\boldsymbol{K}_s$, $\Delta\boldsymbol{r}_{t,t+\Delta t}$ - unknown increment of the generalized displacement vector.

Unknown values of displacements, displacement rates and accelerations at the following instants $t,\ t+\Delta t$, are determined by the incremental expressions:

$$\boldsymbol{r}_{t+\Delta t} = \boldsymbol{r}_t + \Delta\boldsymbol{r}_{t,t+\Delta t},\ \ \dot{\boldsymbol{r}}_{t+\Delta t} = \dot{\boldsymbol{r}}_t + \Delta\dot{\boldsymbol{r}}_{t,t+\Delta t},\ \ \ddot{\boldsymbol{r}}_{t+\Delta t} = \ddot{\boldsymbol{r}}_t + \Delta\ddot{\boldsymbol{r}}_{t,t+\Delta t}. \tag{4.2}$$

The vector of generalized external loading is determined in the analogical, incremental way:

$$\boldsymbol{R}_{t+\Delta t} = \boldsymbol{R}_t + \Delta\boldsymbol{R}_{t,t+\Delta t} \tag{4.3}$$

In turn, the vector of generalized nodal forces, which corresponds to stress state at the instant $t + \Delta t$, has the form:

$$\boldsymbol{F}_t = \boldsymbol{R}_t - \boldsymbol{M}\ddot{\boldsymbol{r}}_t \equiv \boldsymbol{F}_{t-\Delta t} + \Delta\boldsymbol{F}_{t-\Delta t,t} \tag{4.4}$$

The system of equations of motion (4.1) is solved by means of the implicit numerical integration procedure, known as the Newmark method [11]. Using this procedure enables the iterative solving of equations system with application of the modified Newton-Raphson method [11].

5. NUMERICAL ANALYSIS OF REINFORCED CONCRETE DEEP BEAM

Rectangular reinforced concrete deep beam with orthogonal reinforcement system, marked by Leonhardt and Walther in the report [5] as a test specimen WT3, was selected to numerical analysis, Fig. 2b. There are following dimensions of the deep beam: length and depth $L = H = 160\ cm$, thickness $t = 10\ cm$. The main reinforcement was made from steel of $A - III$ grade ($f_y = 410\ MPa$) or $A - H$ grade ($f_y = 690\ MPa$), in the form of 4 layers of reinforcement loops with bar diameter $\emptyset 8\ mm$ and laid at the bottom area of the beam. Upper areas of the beam are reinforced by vertical and horizontal stirrups made from steel of $A - I$ grade ($f_y = 240\ MPa$), with bar diameter $\emptyset 5\ mm$ and $s = 26\ cm$ spacing.

Behavior of presented reinforced concrete deep beam was analyzed under uniformly distributed on the top edge, permanent in the time, impulsive type of load $p(t) = p = const.$, of different load level parameter $\alpha = P/P_o$, where $P = p \times L$ is total loading and P_o is the estimation of the static load-carrying capacity obtained in the numerical solutions.

To illustrate the impact of high-strength concrete on the dynamic load capacity of rectangular reinforced concrete deep beams, numerical experiments were carried out for a beam with the reinforcement arranged like in experiment [5] and with modified parameters describing the constitutive model of concrete (concrete grade *C100, C200, C300*). Additionally, the impact of changing the strength parameters of the reinforcing steel, i.e. the impact of swapping $A - III$ ordinary steel, similarly to experiment [5], for $A - H$ steel with increased strength, was analyzed. For that purpose, the point x_b in the mid-span of the bottom edge (designated in Fig. 2a) was adopted for the observation of dynamic changes of displacement of the deep beam. Moreover, the following points x_2 , x_4 , x_6 , x_8 , x_{10} , x_{12} , x_{14} , x_{16} , $x_{18} = x_b$ were selected for observation in order to illustrate the variability over time of the bottom edge of the deep beam, Fig. 2a.

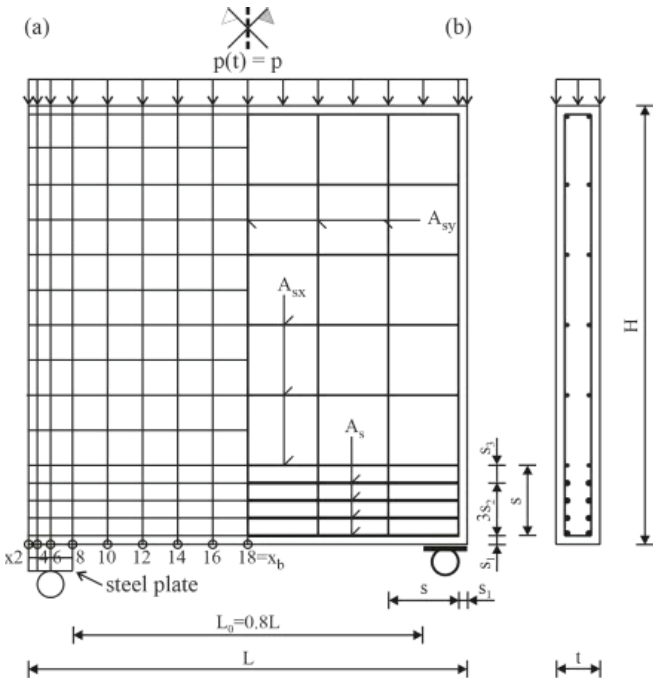

Fig. 2. Finite element mesh (a) of reinforced concrete deep beam (b) under dynamic loading

($A_{sx} = 6 \times 2\emptyset5\ A-I$, $A_{sy} = 7 \times 2\emptyset5\ A-I$, $A_s = 4 \times 2\emptyset8\ A-III\ /\ A-H$
$s = 26\ cm$, $s_1 = s/13$, $s_2 = 3s_1$, $s_4 = 4s_1$)

However, at first the influence of very high strength of structural materials was tested to estimate of the static load - carrying capacity of the deep beam.

Fig. 3 and 4 present graphs of the relationship of vertical displacement υ_b of a point x_b as a function of static load level $\alpha = P_{0(i)}/P_{(1)}$. To compare the results, studies containing: experimental results of Leonhardt, Walther (1), solutions according to the proposed method for ordinary concrete *C30* marked by (2), solutions for very high strength concretes and for ordinary steel *A-III* marked by (3), (4), (5) are presented in the Fig. 3, while solutions for concretes with very high strength and for steels with increased strength *A-H* marked by (6), (7), (8) are shown in the Fig. 4.

As the results, the estimation of the static load-carrying capacity was obtained in numerical solutions:

- for concretes *C100, C200, C300* and steel $A-III$: $P_0 = \{2210\ \text{kN}, 2595\ \text{kN}, 3317\ \text{kN}\}$,
- for concretes *C100, C200, C300* and steel $A-H$: $P_0 = \{2085\ \text{kN}, 3028\ \text{kN}, 3999\ \text{kN}\}$.

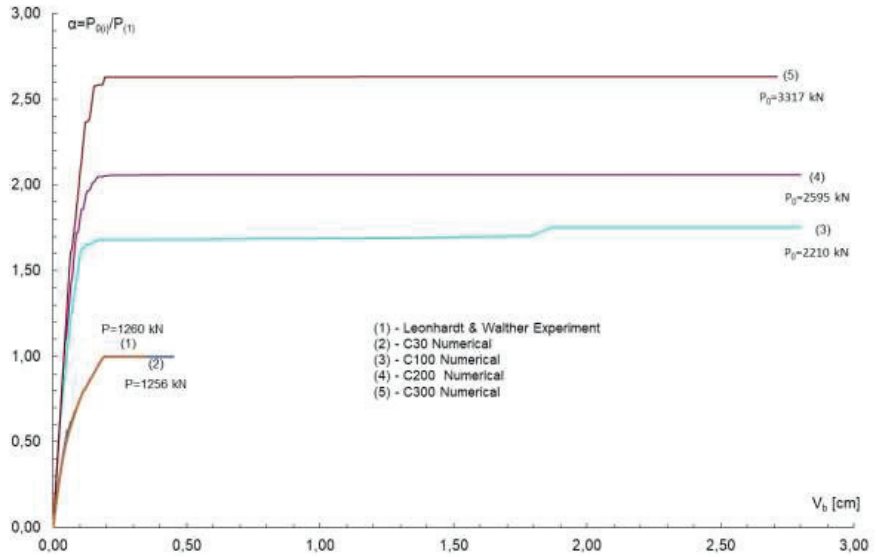

Fig. 3. Displacement of the midpoint x_b at the bottom edge of the deep beam vs. static load level relationship for reinforcing steel of $A-III$ grade

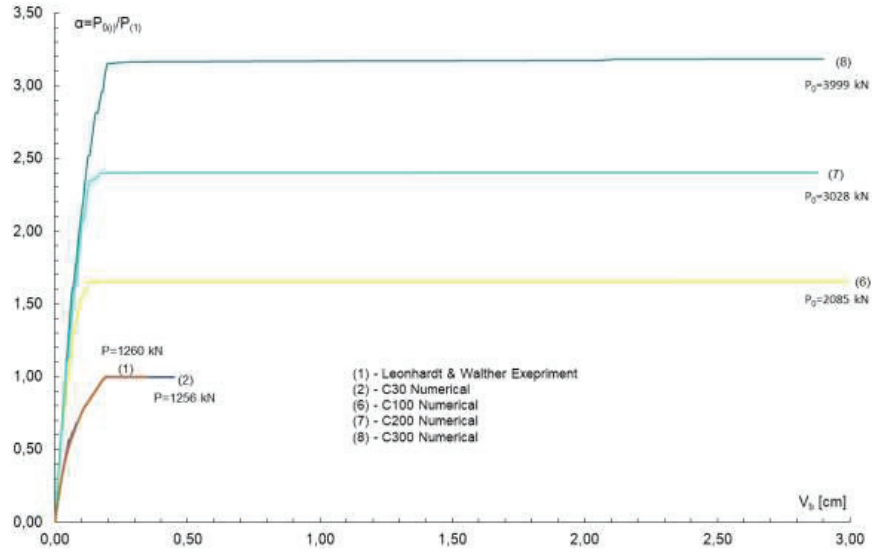

Fig. 4. Displacement of the midpoint x_b at the bottom edge of the deep beam vs. static load level relationship for reinforcing steel of $A-H$ grade

Fig. 5 shows variation in time of vertical displacement v_b in point x_b at the bottom edge for the load level $\alpha = P/P_{o(i)} = 0.5$ for the concretes of *C100, C200, C300* grades, and reinforced by steel of $A - III$ grade. The load level $\alpha = 0.5$ is the maximum load level at which stabile vibrating motion is still observed around the equilibrium level corresponding to the permanent displacements. After exceeding this load level (i.e. for $\alpha = 0.6$) the lack of stabile oscillations around the equilibrium level is observed in Fig. 6 for all the types of deep beams, and as a consequence, the infinitely large increments of vertical displacements appear as a destruction symptom of the deep beams destruction. Therefore, the load level $\alpha = 0.5$ determines the level of the dynamic load capacity of the deep beams, determined with the accuracy to the value of load step.

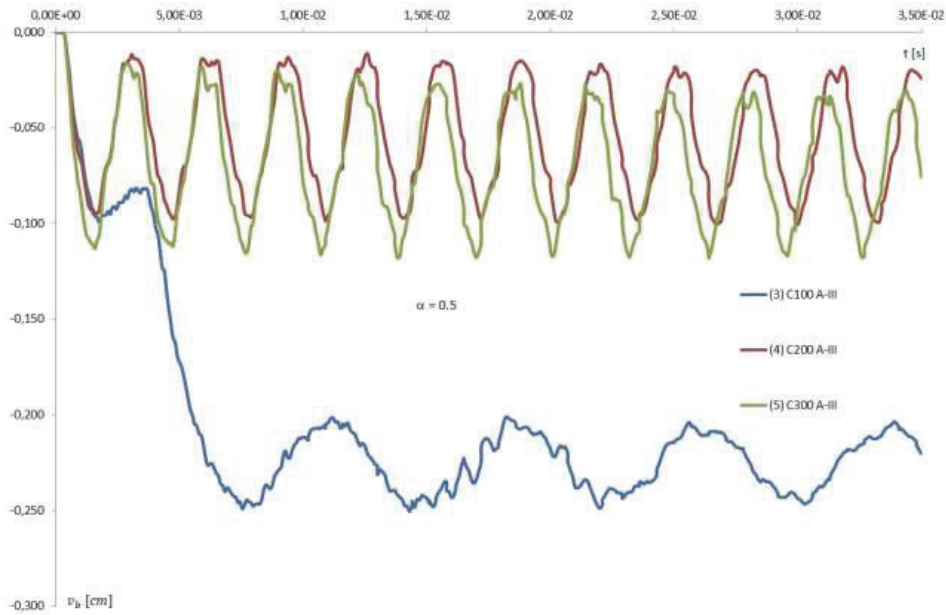

Fig. 5. Variation in time of displacement of midpoint x_b at the bottom edge for load level $\alpha = 0.5$

Fig. 7 shows variation in time of vertical displacement v_b in point x_b at the bottom edge for the load levels $\alpha = 0.4$, $\alpha = 0.5$, $\alpha = 0.6$ for the concretes of *C200, C300, C100* grades respectively, and reinforced by steel of $A - H$ grade. The load levels $\alpha = 0.4$, $\alpha = 0.5$, $\alpha = 0.6$ are the maximum load levels at which vibrating motion are still observed around the equilibrium levels corresponding to the permanent displacements.

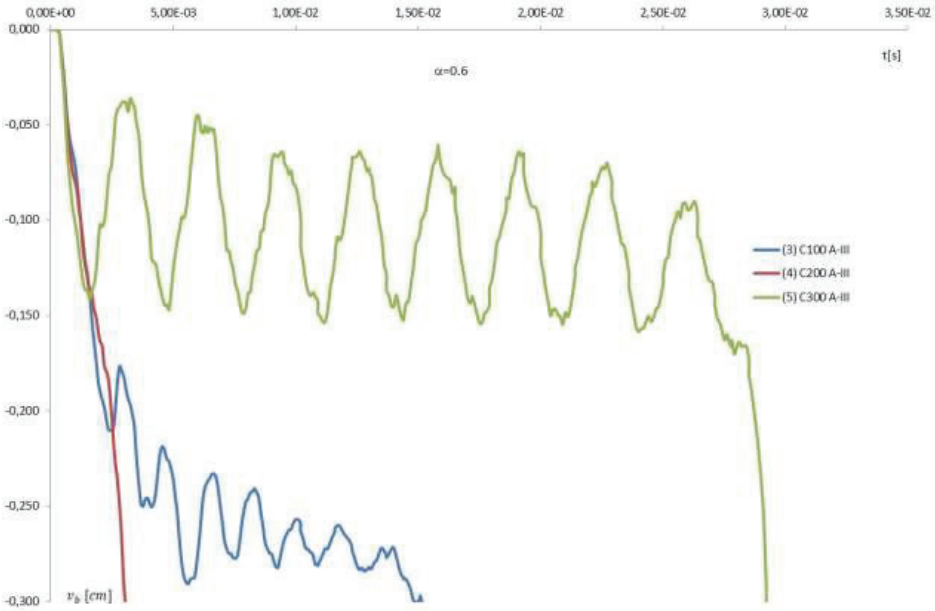

Fig. 6. Variation in time of displacement of midpoint x_b at the bottom edge for load level $\alpha = 0.6$

After exceeding these load levels (i.e. for $\alpha = 0.5$, $\alpha = 0.6$, $\alpha = 0.7$) the lack of stabile oscillations around the equilibrium level are observed in Fig. 8 for all types of the deep beams. Then, the infinitely large increments of vertical displacements appear as a destruction symptom of the deep beams' destruction. The load levels $\alpha = 0.4$, $\alpha = 0.5$, $\alpha = 0.6$ can be recognized as the levels of the dynamic load capacity of the deep beams, determined with the accuracy to the value of load step. Fig. 9 shows the variability of the permanent dynamic vertical displacement in selected points in the bottom edge of the *C100/A-III* deep beam under various load levels $\alpha = P/P_{0(3)}$. Within the structure's elastic capacity range, at load levels of $\alpha = 0.1$ and $\alpha = 0.2$, the maximum permanent displacement occurred in the span at point $x_{18} = x_b$ and the observed amplitude values of vertical displacements decreased monotonically towards the support. The same behavior of the structure was observed at a load level of $\alpha = 0.3$, when cracking of the concrete in the vicinity of the support occurred. At the load level of $\alpha = 0.4$, a sudden increase in the displacement of point x_{10} can be observed, below the value of displacement of points in the vicinity of the central axis of the vertical symmetry. It is caused by the development of the area of cracked concrete in the vicinity of that point – a propagation of the cracked area occurred in the vertical direction. Upon the further increase of load level to $\alpha = 0.5$, stabilization of displacement of point x_{10} is observed.

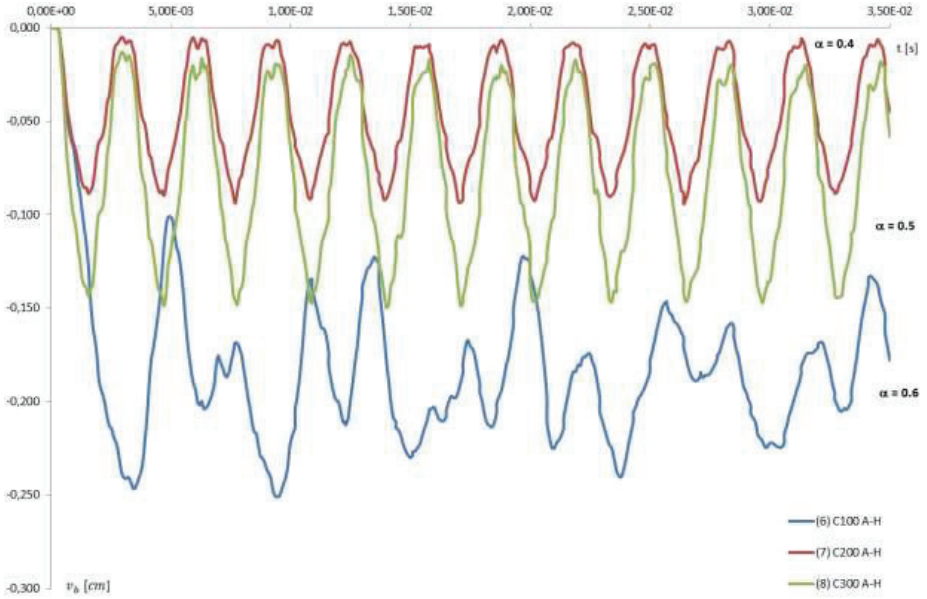

Fig. 7. Variation in time of displacement of midpoint x_b at the bottom edge for the load levels preceding the destruction phase

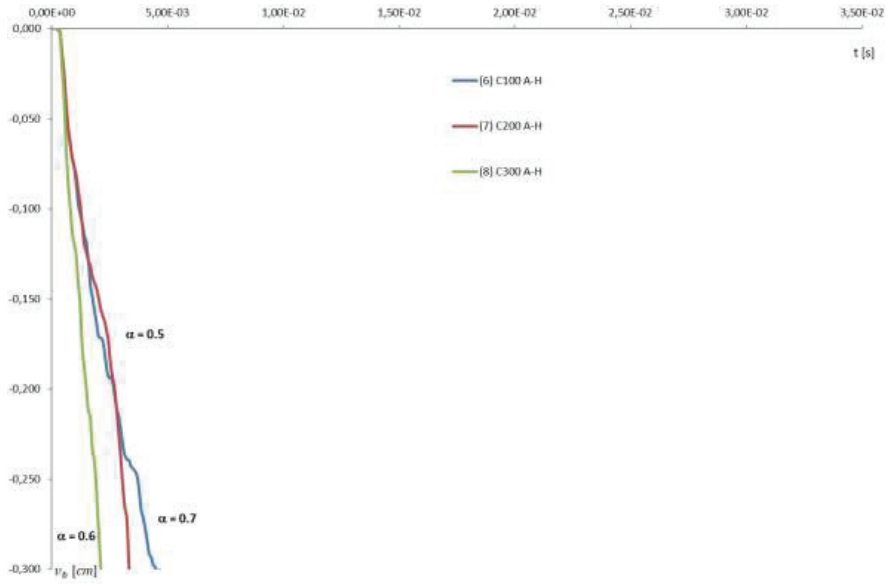

Fig. 8. Variation in time of displacement of midpoint x_b at the bottom edge for the load levels corresponding to the destruction phase

At the same time, a sudden increase in permanent vertical displacements can be observed in the following points x_{12} , x_{14} , x_{16} , $x_{18} = x_b$ in relation to appearance of a new crack areas in the central section and with the change of propagation of cracked area in the shear zone from vertical to diagonal towards to the central section. Under the load level of $\alpha = 0.6$, an unlimited increase of vertical displacements occurred successively in points x_{16} , x_{18} , x_{16} which is a clear sign of the exhaustion of the load - carrying capacity and destruction of the deep beam.

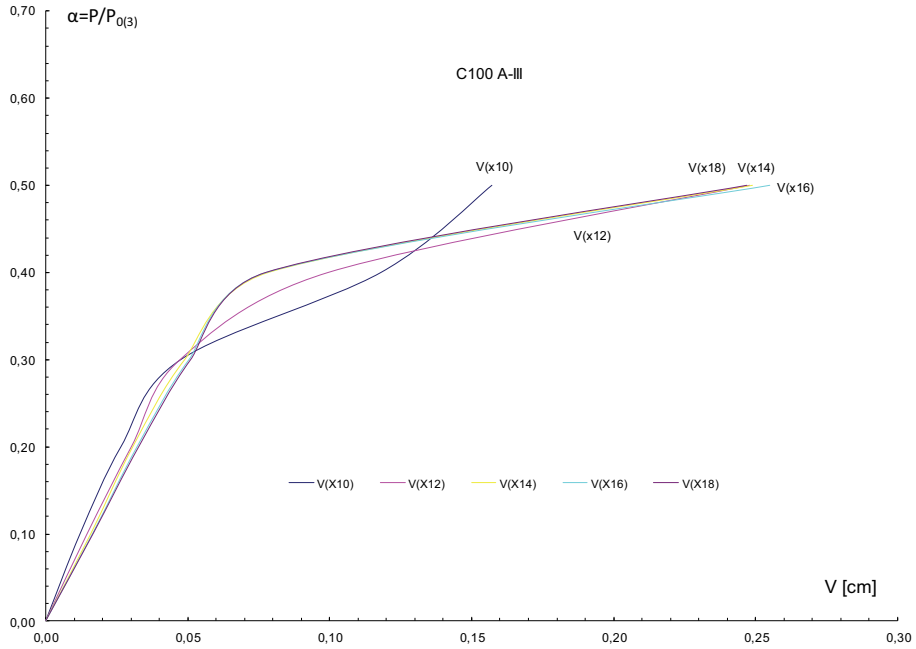

Fig. 9. Permanent displacement of the points at the bottom edge vs. load level relationship for the *C100/A-III* deep beam

Fig. 10 shows the variability of the permanent vertical displacement in selected points in the *C300/A-III* deep beam's bottom edge under various loads levels $\alpha = P/P_{0(5)}$. In the range of elastic capacity of the structure, the load levels of $\alpha = 0.1$ and $\alpha = 0.2$ gave the maximum permanent deflection, just like in the *C100* concrete deep beam's mid-span at point $x_{18} = x_b$ and the observed amplitude values of the vertical displacements decreased monotonically towards to the support. The same behavior of the structure was observed at the load level of $\alpha = 0.3$, when the cracking of the concrete in vicinity of the support occurred. As the load level was increased to

$\alpha = 0.4$, cracks propagation occurred of the partially cracked areas, i.e. in the shear zone only, but in the vertical upward direction only - which resulted in a decrease in the permanent vertical displacement in the points in the middle cross-section's vicinity, i.e. at points x_{16} and x_{18}. At the load level of $\alpha = 0.5$, the previous relation type of was observed: the maximum permanent displacement was at point x_{18} of the mid-span at lower load levels, and the observed vertical displacements decreased monotonically towards to the support. At the load level of $\alpha = 0.5$, no concrete cracks were appeared in the middle cross-section. Whereas at the load level of $\alpha = 0.6$, further development of the cracked concrete area was visible. There was an unlimited increase of vertical displacements at the points adjacent to the mid-span cross-section which indicates on the deep beam's carrying capacity exhaustion and progressive destruction.

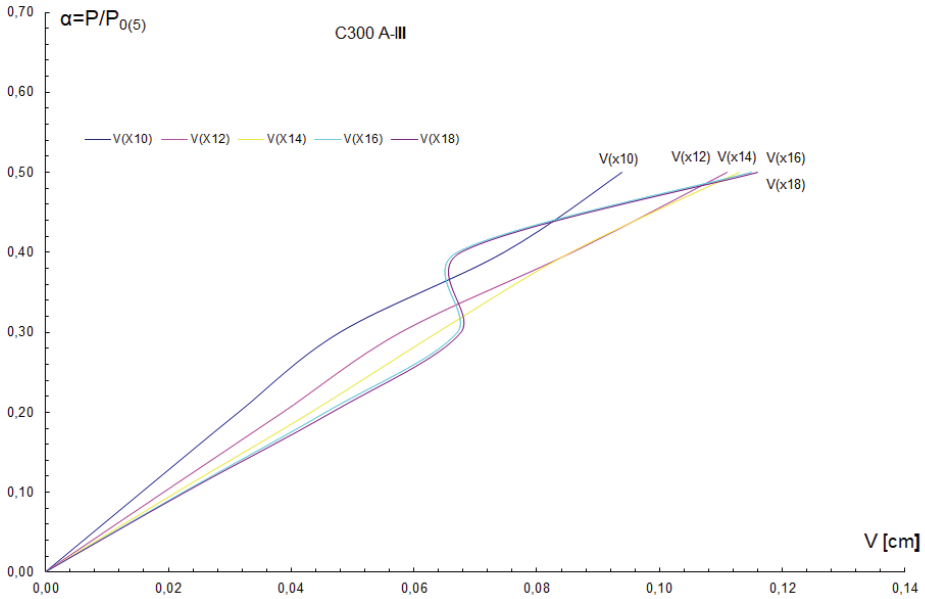

Fig. 10. Permanent displacement of the points at the bottom edge vs. load level relationship for the *C100/A-III* deep beam

Fig. 11 shows the variability of the permanent vertical displacement in the selected points in the *C100/A-H* deep beam's bottom edge under various loads level $\alpha = P/P_{0(6)}$. In the range of elastic capacity of the structure, the load levels $\alpha = 0.1$ and $\alpha = 0.2$ gave the maximum displacement, just like in the *C100/A-III* deep beam, in the mid-span at point $x_{18} = x_b$, and the observed amplitude

values of the vertical displacements decreased monotonically towards to the support. Also, at the load level $\alpha = 0.3$, the same behavior of the structure can be observed, when cracking of the concrete in the vicinity of the support occurred. At the load level of $\alpha = 0.4$, just like in the *C100/A-III* deep beam, a sudden increase in the permanent vertical displacement of point x_{10} occurs, exceeding the values of displacements of points adjacent to the central axis of the vertical symmetry. It is caused by the development of an area of cracked concrete in the vicinity of this point - a propagation of the cracked area occurred in the vertical direction.

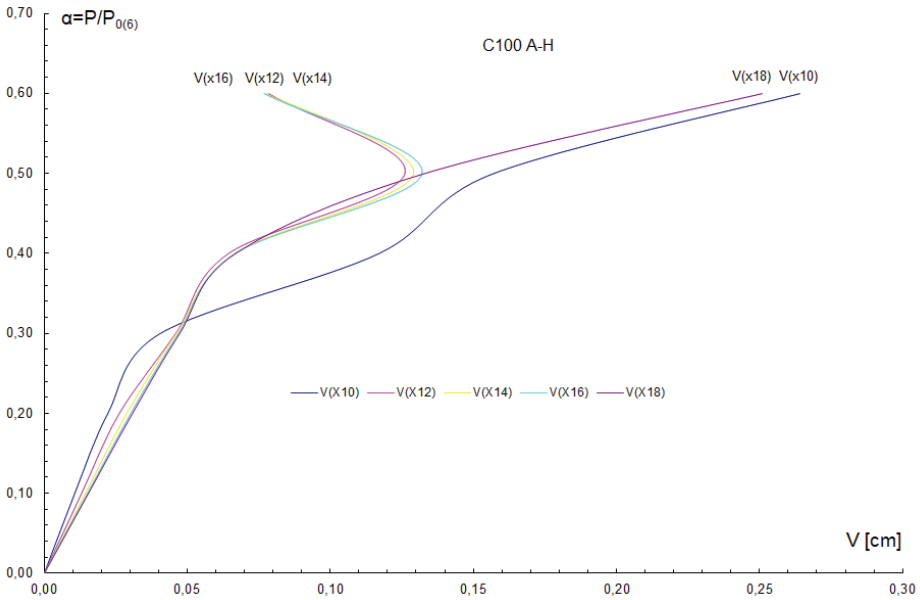

Fig. 11. Permanent displacement of the points at the bottom edge vs. load level relationship for the *C100/A-H* deep beam

Upon a further increase of load level to $\alpha = 0.5$, stabilization of parameter displacement of point x_{10} is observed. At the same time, an increase in displacements can be observed in the following points $x_{12}, x_{14}, x_{16}, x_{18} = x_b$ close to the middle cross-section - this increase, however, is significantly smaller than in the case of the *C100/A-III* deep beam. It is caused by the difference in the development of concrete crack areas. Currently, just as in the deep beam reinforced with *A-III* steel, a change occurred in the direction of propagation of the cracked area in the shear zone from vertical to diagonal towards to the central section, however, unlike in the deep beam reinforced with

A-III steel, concrete cracking in the lower layers of the central section did not occur. Only at the load level of $\alpha = 0.6$, a sudden increase of vertical displacements was observed, however, only from point x_{18} in the middle cross-section because of the appearance of a new crack area in the middle cross-section (vertical crack) and its sudden development in the vertical direction. At the same time, a further increase in the vertical displacements of point x_{10} is observed and a decrease in the permanent vertical displacements of points x_{12}, x_{14} and x_{16}, being a symptom of the deep beam's local load-carrying capacity reduction. The observed changes of the permanent displacements of the selected points indicate an evident change of the mechanism of the deep beam's cracks and stress/strain states caused by the replacement of *A-III* reinforcing steel by *A-H* steel. For a load level of $\alpha = 0.7$, an unlimited increase in vertical displacements was observed successively at points x_{12}, x_{14}, x_{16} and $x_{18} = x_b$. It is an obvious sign of the exhaustion of load-carrying capacity and destruction of the deep beam, however, at a different, higher load level than in the deep beam reinforced with *A-III* steel.

6. CONCLUSIONS

Analysis of dynamic load-carrying capacity of inelastic reinforced concrete deep beam as a function of two factors - strength of concrete and yield limit of reinforcement steel – determining the effort level of structural element was presented in the paper. Special grades of concrete of very high strength were considered. The analysis regarding such the grades of concrete have required introducing the modification of the parameters of the constitutive model of material.

Low increase of dynamic load-carrying capacity of deep beam being out-of-proportion to increasing the strength of concrete and yield limit of reinforcing steel was stated in the numerical analysis. Such a limited effect is the symptom of the specific changes of effort mechanism as well as concentration of cracking and crushing zones in the concrete. Increasing of the yield limit of main reinforcing steel does not lead to the considerable increase of the dynamic load-carrying capacity of deep beam.

The further research intention of the authors consists in enhance of the model to description of the finite deformations and demonstrating the full capabilities of the computational model, based on comparisons to experimental results of dynamically loaded deep beams.

REFERENCES

1. G. Bąk and A. Stolarski, Delayed yield effect in dynamic flow of elastic/visco-perfectly plastic material, Arch. Mech., 37, 4-5, 285-302, 1985.
2. J. D. Campbell, The dynamic yielding of mild steel, Acta Metallurgica, 1, 706-710, 1953.
3. W. Cichorski and A. Stolarski, Modelling of inelastic behaviour of reinforced concrete deep beam. Journal of Achievements in Materials and Manufacturing Engineering, 74 (1), 2016, 37-44.
4. W. Cichorski and A. Stolarski, The analysis of the displacement state of the inelastic reinforced concrete deep beam under static load, 2001, Bulletin of the Military University of Technology, L, 5(585), 2001, 5-20, (in Polish).
5. F. Leonhardt and R. Walther, Wandartige träger, Report, Deutscher Asschüβ für Stahlbeton, 229, Berlin, Germany, 1966.
6. P. Perzyna, The constitutive equations for rate sensitive plastic materials, Quart. Appl. Math., 20. 1963, 321-332.
7. A. Stolarski and W. Cichorski. Influence of high strength of concrete and reinforcing steel on behaviour of r/c deep beam, Archives of Civil Engineering, XLXIX, 2, 2003, 113-130.
8. A. Stolarski and W. Cichorski, The method of analysis of the inelastic behaviour of the reinforced concrete deep beam under static load, Bulletin of the Military University of Technology, 2000, 10(578), 5-30, (in Polish).
9. A. Stolarski, Model of dynamic deformation of concrete, Archives of Civil Engineering, XXXVII, 3-4, 405-447, 1991, (in Polish).
10. A. Stolarski, Dynamic strength criterion for concrete, Journal of Engineering Mechanics, ASCE, vol. 130, 12, 2004, 1428-1435.
11. P. Wriggers, Nonlinear Finite Element Methods, Springer, 2008.
12. A. Stolarski, W. Cichorski, A. Szcześniak, Non-Classical Model of Dynamic Behaviour of Concrete, Applied Sciences, 2019, 9(13), 2590; doi:10.3390/app9132590.
13. I. Marzec, J. Tejchman, A. Winnicki, Computational simulations pf concrete behavior under dynamic conditions using elasto-visco-plastic model with non-local softening, Computers and Concrete, 105, Vol. 15, No. 4 (2015), 515-545: doi: http://dx.doi.org/10.12989/cac.2015.15.4.515.
14. A. Wosatko, A. Genikomsou, J. Pamin, M. A. Polak, A. Winnicki, Examination of two regularized damage-plasticity models for concrete with regard to crack closing, Engineering Fracture Mechanics, 2018, 190-211.

LIST OF FIGURES:

Fig. 1. Interpretation of material parameters describing constitutive model of concrete

Rys. 1. Interpretacja stałych materiałowych opisujących model konstytutywny betonu

Fig. 2. Finite element mesh (a) of reinforced concrete deep beam (b) under dynamic loading

($A_{sx} = 6 \times 2\emptyset5\ A-I$, $A_{sy} = 7 \times 2\emptyset5\ A-I$, $A_s = 4 \times 2\emptyset8\ A-III\ /\ A-H$

$s = 26\ cm$, $s_1 = s/13$, $s_2 = 3s_1$, $s_4 = 4s_1$)

Rys. 2. Siatka elementów skończonych (a) żelbetowej tarczy (b) pod obciążeniem dynamicznym

($A_{sx} = 6 \times 2\emptyset5\ A-I$, $A_{sy} = 7 \times 2\emptyset5\ A-I$, $A_s = 4 \times 2\emptyset8\ A-III\ /\ A-H$

$s = 26\ cm$, $s_1 = s/13$, $s_2 = 3s_1$, $s_4 = 4s_1$)

Fig. 3. Displacement of the midpoint x_b at the bottom edge of the deep beam vs. static load level relationship for reinforcing steel of $A-III$ grade

Rys. 3. Przemieszczenie punktu środkowego x_b na dolnej krawędzi tarczy w zależności od poziomu statycznego obciążenia dla stali zbrojeniowej $A-III$

Fig. 4. Displacement of the midpoint x_b at the bottom edge of the deep beam vs. static load level relationship for reinforcing steel of $A-H$ grade

Rys. 4. Przemieszczenie punktu środkowego x_b na dolnej krawędzi tarczy w zależności od poziomu statycznego obciążenia dla stali zbrojeniowej $A-H$

Fig. 5. Variation in time of displacement of midpoint x_b at the bottom edge for load level $\alpha = 0.5$

Rys. 5. Zmiana przemieszczenia w czasie punktu środkowego x_b na dolnej krawędzi dla poziomu obciążenia $\alpha = 0.5$

Fig. 6. Variation in time of displacement of midpoint x_b at the bottom edge for load level $\alpha = 0.6$

Rys. 6. Zmiana przemieszczenia w czasie punktu środkowego x_b na dolnej krawędzi dla poziomu obciążenia $\alpha = 0.6$

Fig. 7. Variation in time of displacement of midpoint x_b at the bottom edge for the load levels preceding the destruction phase

Rys. 7. Zmiana przemieszczenia w czasie punktu środkowego x_b na dolnej krawędzi dla poziomów obciążenia poprzedzających zniszczenie

Fig. 8. Variation in time of displacement of midpoint x_b at the bottom edge for the load levels corresponding to the destruction phase

Rys. 8. Zmiana przemieszczenia w czasie punktu środkowego x_b na dolnej krawędzi dla poziomów obciążenia odpowiadających fazie zniszczenia

Fig. 9. Permanent displacement of the points at the bottom edge vs. load level relationship for the *C100/A-III* deep beam

Rys. 9. Zależność trwałych przemieszczeń punktów na dolnej krawędzi od poziomu obciążenia dla tarczy *C100/A-III*

Fig. 10. Permanent displacement of the points at the bottom edge vs. load level relationship for the *C100/A-III* deep beam

Rys. 10. Zależność trwałych przemieszczeń punktów na dolnej krawędzi od poziomu obciążenia dla tarczy *C300/A-III*

Fig. 11. Permanent displacement of the points at the bottom edge vs. load level relationship for the *C100/A-H* deep beam

Rys. 11. Zależność trwałych przemieszczeń punktów na dolnej krawędzi od poziomu obciążenia dla tarczy *C100/A-H*

LIST OF TABLES:

PROGNOZA DYNAMICZNEGO ZACHOWANIA TARCZ ŻELBETOWYCH Z MATERIAŁÓW BARDZO WYSOKIEJ WYTRZYMAŁOŚCI

Słowa kluczowe: mechanika konstrukcji, konstrukcje żelbetowe, tarcze, dynamika, nieliniowość fizyczna

PODSUMOWANIE:

W pracy przedstawiono prognozę zachowania prostokątnych tarcz żelbetowych wykonanych z betonów o bardzo wysokiej wytrzymałości obciążonych dynamicznie z uwzględnieniem fizycznych nieliniowości materiałów konstrukcyjnych: betonu i stali zbrojeniowej.

Do opisu dynamicznych właściwości materiałów konstrukcyjnych dla betonu zastosowano niestandardowy model deformacji dynamicznej uwzględniający wytrzymałość dynamiczną betonu, osłabienie materiałowe, zarysowanie i miażdżenie betonu. W modelu opisującym dynamiczne zachowanie betonu dokonano modyfikacji paramentów materiału uwzględniających charakterystykę naprężeniowo-odkształceniową uwzgledniająca parametry betonu bardzo wysokiej wytrzymałości. Dla stali zbrojeniowej przyjęto model sprężysto/lepko-idealnie plastycznego materiału z uwzględnieniem efektu opóźniania plastycznego. Modelowanie procesów dynamicznego odkształcania płaskiego ustroju konstrukcyjnego- tarczy żelbetowej przeprowadzono przy użyciu własnych procedur numerycznych i programów obliczeniowych bazując na metodzie elementów skończonych.

W pracy przestawiono analizę porównawczą wyników rozwiązań numerycznych dla tarczy żelbetowej, która była przedmiotem statycznych badań doświadczalnych Leonhardta i Walthera [5]. Żelbetowa tarcza o ortogonalnym układzie zbrojenia będąca przedmiotem badań doświadczalnych [5] wykonana była z betonu klasy $C30$ i zbrojona stalą zwykłą klasy *A-III*. W ramach doświadczenia numerycznego przeanalizowano zachowanie analogicznych tarcz żelbetowych

o ortogonalnym układzie zbrojenia, ale wykonanych z betonu wysokiej wytrzymałości *C100*, *C200* i *C300* zbrojonych w 2 wariantach – analogicznie jak w doświadczeniu [5] stalą zwykłą klasy *A-III* oraz stalą o podwyższonej wytrzymałości klasy *A-III*. Analizowane tarcze obciążono w sposób dynamiczny. Dokonano analizy stanu przemieszczenia dla wszystkich rodzajów tarcz, przy różnych poziomów obciążenia, aż do osiągnięcia stanu wyczerpania dynamicznej nośności. Przedstawiono wyniki rozwiązań numerycznych ze szczególnym uwzględnieniem wpływu bardzo wysokiej wytrzymałości betonu i stali na przemieszczenia tarczy żelbetowej. Oszacowano dynamiczną nośność prostokątnych tarcz żelbetowych w funkcji dwóch zmiennych parametrów: wytrzymałości betonu oraz wytrzymałości stali zbrojeniowej. W analizie numerycznej stwierdzono nieproporcjonalny przyrost nośności analizowanej tarczy żelbetowej w porównaniu zarówno z przyrostem wytrzymałości betonu jak i stali zbrojeniowej. Wykazano poprawność przyjętych założeń i modeli odkształcenia betonu i stali oraz efektywność metody analizy proponowanej dla problemów numerycznej symulacji zachowania tarcz żelbetowych. Prezentowane wyniki potwierdzają konieczność prowadzenia dalszych badań wpływu paramentów modelu konstytutywnego betonu o bardzo wysokiej wytrzymałości na mechanizm zniszczenia i wytężenia elementów żelbetowych. Pełna analiza wpływu innych czynników, takich jak układ geometryczny, stopień zbrojenia i wytrzymałość stali zbrojeniowej, decydujących o nośności elementów żelbetowych, umożliwi ocenę celowości projektowania takich elementów z zastosowaniem wysoko wytrzymałościowych materiałów konstrukcyjnych.

Received 11.09.2019, Revised 29.11.2019